PHYSICAL REVIEW D **87,** 035027 (2013)

# First lower limits on the photon-axion-like particle coupling from very high energy gamma-ray observations

Manuel Meyer,* Dieter Horns, and Martin Raue

*Institut für Experimentalphysik, Universität Hamburg, Luruper Chaussee 149, 22761 Hamburg, Germany*

(Received 23 November 2012; published 22 February 2013)

The intrinsic flux of very high-energy (VHE, energy $\gtrsim 100$ GeV) $\gamma$ rays from extragalactic sources is attenuated due to pair production in the interaction with photons of the extragalactic background light (EBL). Depending on the distance of the source, the Universe should be opaque to VHE photons above a certain energy. However, indications exist that the Universe is more transparent than previously thought. A recent statistical analysis of a large sample of VHE spectra shows that the correction for absorption with current EBL models is too strong for the data points with the highest attenuation. An explanation might be the oscillation of VHE photons into hypothetical axionlike particles (ALPs) in ambient magnetic fields. This mechanism would decrease the opacity, as ALPs propagate unimpeded over cosmological distances. Here, a large sample of VHE $\gamma$-ray spectra obtained with imaging air Cherenkov telescopes is used to set, for the first time, lower limits on the photon-ALP coupling constant $g_{a\gamma}$ over a large range of ALP masses. The conversion in different magnetic field configurations, including intracluster and intergalactic magnetic fields together with the magnetic field of the Milky Way, is investigated, taking into account the energy dependence of the oscillations. For optimistic scenarios of the intervening magnetic fields, a lower limit on $g_{a\gamma}$ of the order of $10^{-12}$ GeV$^{-1}$ is obtained, whereas more conservative model assumptions result in $g_{a\gamma} \gtrsim 2 \times 10^{-11}$ GeV$^{-1}$. The latter value is within reach of future dedicated ALP searches.

DOI: 10.1103/PhysRevD.87.035027 PACS numbers: 14.80.Va, 95.85.Pw, 98.54.Cm, 98.70.Vc

## I. INTRODUCTION

Very high-energy (VHE, energy $\gtrsim 100$ GeV) $\gamma$ rays from extragalactic sources interact with photons of the extragalactic background light (EBL) and produce $e^+e^-$ pairs [1–3]. As a result, the intrinsic $\gamma$-ray flux is exponentially suppressed with the optical depth, $\tau(z, E)$, that increases with both the redshift $z$ of the source and energy $E$. Above a certain energy, the Universe should thus become opaque to $\gamma$ rays from sufficiently distant sources. The optical depth also depends on the photon number density of the EBL, whose exact level remains unknown, as direct observations are difficult due to contamination by foreground emission [4]. The EBL ranges from ultraviolet (UV)/optical to far-infrared wavelengths and originates from the starlight integrated over all epochs and the starlight absorbed and reemitted by dust in galaxies (see, e.g., Refs. [5,6] for a review). Nevertheless, firm lower limits in the optical and infrared exist which can be derived from galaxy number counts [7,8], and recent EBL models show a good agreement in the overall shape of the spectrum (e.g., Refs. [9–11]). In addition, VHE $\gamma$-ray spectra from extragalactic sources can be used to place upper limits on the EBL density if certain assumptions about the intrinsic spectra are made (see, e.g., Refs. [12,13] for recent upper limits).

However, indications have been found that the Universe is more transparent to VHE $\gamma$ rays than the prediction of EBL models suggests (e.g., Refs. [14–17]). The authors of Ref. [18] introduced a nonparametric test to quantify the accordance between EBL model predictions and VHE observations. They tested the EBL model of Ref. [10] (henceforth the KD model), which is designed to produce a minimal attenuation as it closely follows the galaxy number counts in the infrared. The authors used a statistical sample of the spectra of active galactic nuclei (AGNs) measured with imaging air Cherenkov telescopes (IACTs) and fitted analytical functions to the spectral points [19]. Subsequently, the authors tested if the residuals of data points that correspond to an optical depth $\tau \geq 2$ follow the expectation to scatter around a zero mean. They found, though, that the mean is larger than zero at a $\sim 4\sigma$ significance level, indicating an overcorrection of the data with the KD model. A possible solution to this observed pair production anomaly might be the conversion of photons into axionlike particles (ALPs) [16,17]. ALPs are pseudo-Nambu-Goldstone bosons that are created if additional global symmetries to the standard model are spontaneously broken (see, e.g., Ref. [20] for a review). Such fields are a common prediction in compactified string theories [21]. Their phenomenology is closely related to that of axions, which solve the strong *CP* problem in QCD [22–24]. Most importantly in the present context, ALPs share the same coupling to photons as axions, characterized by the Lagrangian

$$\mathcal{L}_{a\gamma} = \frac{1}{4} g_{a\gamma} \tilde{F}_{\mu\nu} F^{\mu\nu} a = g_{a\gamma} \mathbf{E} \cdot \mathbf{B} a, \qquad (1)$$

*manuel.meyer@physik.uni-hamburg.de

 

where $F^{\mu\nu}$ is the electromagnetic field tensor (with electric and magnetic fields $\mathbf{E}$ and $\mathbf{B}$, respectively), $\tilde{F}^{\mu\nu}$ is its dual, $a$ is the ALP field strength, and $g_{a\gamma}$ is the photon-ALP coupling strength which has the dimension $(\text{Energy})^{-1}$. In contrast to the axion, the ALP mass $m_a$ is unrelated to the coupling strength.

The effect of photon-ALP mixing on VHE $\gamma$-ray spectra in different magnetic field settings has been extensively discussed in the literature. The case of a conversion in an intergalactic magnetic field (IGMF) was addressed by, e.g., Refs. [16,17,25–27]. The authors of, e.g., Refs. [28,29] included the magnetic fields in and around the source, and in Ref. [30] the backconversion of ALPs into photons in the galactic magnetic field (GMF) of the Milky Way was studied. Recently, the photon-ALP mixing for sources located inside galaxy clusters and the reconversion in the GMF was also investigated [31]. Usually, previous studies used fixed values for the ALP mass and coupling close to current experimental bounds in order to maximize the effect on the $\gamma$-ray spectra.

In this article, the goal is to determine the preferred region in the $(m_a, g_{a\gamma})$ parameter space that minimizes the tension between data and model predictions found in Ref. [18]. This allows, for the first time, to place a lower limit on the photon-ALP coupling to explain the observed transparency of the Universe for VHE $\gamma$ rays. Four different scenarios for the intervening magnetic field will be considered, including mixing in the IGMF, the intracluster magnetic field (ICMF), and the GMF of the Milky Way. In two cases, the parameters of the IGMF and ICMF will be chosen as optimistically as possible in order to derive lower limits on $g_{a\gamma}$. Additionally, a more conservative choice of $B$-field model parameters will be investigated. Furthermore, two different EBL model realizations will be studied.

The paper is organized as follows: In Sec. II, the theory of photon-ALP conversions is briefly reviewed. In Sec. III, the different magnetic field configurations and the scenarios that are analyzed are summarized. Subsequently, the method of constraining the ALP parameter space is laid out in Sec. IV before presenting the actual results in Sec. V and concluding in Sec. VI.

## II. PHOTON-ALP CONVERSION IN MAGNETIC FIELDS

The photon-ALP interaction is described by the Lagrangian

$$\mathcal{L} = \mathcal{L}_{a\gamma} + \mathcal{L}_{\text{EH}} + \mathcal{L}_a, \tag{2}$$

where $\mathcal{L}_a$ is given in Eq. (1), $\mathcal{L}_{\text{EH}}$ is the effective Euler-Heisenberg Lagrangian accounting for one-loop corrections in the photon propagator (see, e.g., Ref. [32]), and $\mathcal{L}_a$ includes the kinetic and mass term of the ALP,

$$\mathcal{L}_a = \frac{1}{2}\partial_\mu a \partial^\mu a - \frac{1}{2} m_a^2 a^2. \tag{3}$$

For a monochromatic photon/ALP beam of energy $E$ propagating along the $x_3$ axis in a cold plasma with a homogeneous magnetic field, it can be shown that $\mathcal{L}$ leads to the following Schrödinger-like equation of motion [32]:

$$\left(i\frac{\mathrm{d}}{\mathrm{d}x_3} + E + \mathcal{M}_0\right)\begin{pmatrix} A_1(x_3) \\ A_2(x_3) \\ a(x_3) \end{pmatrix} = 0, \tag{4}$$

where $A_1(x_3)$ and $A_2(x_3)$ describe the linear photon polarization amplitudes along $x_1$ and $x_3$, respectively, and $a(x_3)$ denotes the ALP field strength. Let $\mathbf{B}_\perp$ denote the magnetic field transverse to the beam propagation direction. If one chooses $\mathbf{B}_T$ to lie only along the $x_2$ direction, the mixing matrix $\mathcal{M}_0$ can be written as

$$\mathcal{M}_0 = \begin{pmatrix} \Delta_{||} & 0 & 0 \\ 0 & \Delta_\perp & \Delta_{a\gamma} \\ 0 & \Delta_{a\gamma} & \Delta_a \end{pmatrix}, \tag{5}$$

where a mixture of the photon polarization states due to Faraday rotation can be safely neglected for the energies considered here. The matrix elements $\Delta_{||} = \Delta_{\text{pl}} + 7/2\Delta_{\text{QED}}$ and $\Delta_\perp = \Delta_{\text{pl}} + 2\Delta_{\text{QED}}$ account for medium effects on the photon propagation, where $\Delta_{\text{pl}} = -\omega_{\text{pl}}/(2E)$ with the plasma frequency of the medium, $\omega_{\text{pl}}$. The plasma frequency is connected to the ambient thermal electron density $n_{\text{el}}$ through $\omega_{\text{pl}} = 3.69 \times 10^{-11}\sqrt{n_{\text{el}}/\text{cm}^{-3}}$ eV. The QED vacuum birefringence effect is included in $\Delta_{\text{QED}} \propto B_\perp^2$. Furthermore, $\Delta_a = -m_a^2/(2E)$, and the photon-ALP mixing is induced by the off-diagonal element $\Delta_{a\gamma} = 1/2 g_{a\gamma} B_\perp$ (see, e.g., Ref. [31] for numerical values in suitable units of the matrix elements). If photons are lost due to the interaction with the EBL, the elements $\Delta_{||,\perp}$ are modified to include a complex absorption term, $\Delta_{||,\perp} \rightarrow \Delta_{||,\perp} + i/(2\lambda_\gamma^{\text{mfp}})$, where $\lambda_\gamma^{\text{mfp}}$ is the mean free path for photons undergoing pair production. Equation (4) is solved with the transfer function $\mathcal{T}(x_3, 0; E)$ with the initial condition $\mathcal{T}(0, 0; E) = 1$. Neglecting the birefringence contribution for a moment, it can be shown that the photon-ALP oscillations become maximal and independent of the energy $E$ and ALP mass $m_a$ for an energy above the critical energy

$$E_{\text{crit}} \equiv E\frac{|\Delta_a - \Delta_{\text{pl}}|}{2\Delta_{a\gamma}} \approx 2.5\frac{|m_a^2 - \omega_{\text{pl}}^2|}{1\ \text{neV}}\left(\frac{g_{a\gamma}}{10^{-11}\ \text{GeV}^{-1}}\right)^{-1}\left(\frac{B_\perp}{1\ \mu\text{G}}\right)^{-1}\ \text{GeV}, \tag{6}$$

which is the so-called strong mixing regime. However, as the goal of this paper is to constrain the $(m_a, g_{a\gamma})$ parameter space, it is generally not the case that the mixing occurs in this regime.

So far, only a polarized photon beam has been considered. As of today, the polarization of VHE $\gamma$ rays cannot be measured, and one has to consider an unpolarized photon beam and reformulate the problem in terms of density matrices. The general polarization matrix is given by

$$\rho(x_3) = \begin{pmatrix} A_1(x_3) \\ A_2(x_3) \\ a(x_3) \end{pmatrix} \otimes \begin{pmatrix} A_1(x_3) & A_2(x_3) & a(x_3) \end{pmatrix}^*, \quad (7)$$

and the equation of motion takes the form of a von Neumann-like equation,

$$i\frac{\mathrm{d}\rho}{\mathrm{d}x_3} = [\rho, \mathcal{M}_0], \quad (8)$$

which is solved by $\rho(x_3, E) = \mathcal{T}(x_3, 0; E)\rho(0)\mathcal{T}^\dagger(x_3, 0; E)$. In the more general case in which $\mathbf{B}_\perp$ has an arbitrary orientation and forms an angle $\psi$ with the $x_2$ axis, the solution can be found via a similarity transformation

$$V(\psi) = \begin{pmatrix} \cos\psi & -\sin\psi & 0 \\ \sin\psi & \cos\psi & 0 \\ 0 & 0 & 1 \end{pmatrix}, \quad (9)$$

so that $\mathcal{M} = V(\psi)\mathcal{M}_0 V^\dagger(\psi)$, and the solution to the modified Eq. (8) is $\mathcal{T}(x_3, 0; E; \psi) = V(\psi)\mathcal{T}(x_3, 0; E) \times V^\dagger(\psi)$. If, moreover, the beam path can be split up into $n$ domains with a constant and homogeneous magnetic field in each domain but a changing orientation (and strength) from one domain to the next, the complete transfer matrix is simply given by the product over all domains,

$$\mathcal{T}(x_{3,n}, x_{3,0}; E; \psi_{n-1}, \ldots, \psi_0) = \prod_{k=0}^{n-1} \mathcal{T}_k(x_{3,k+1}, x_{3,k}; E; \psi_k), \quad (10)$$

with one mixing matrix $\mathcal{M}_k$ for each domain. The transition probability of observing a photon/ALP beam in the state $\rho_{\mathrm{final}}$ after the crossing of $n$ magnetic domains reads

$$P_{\mathrm{final}} = \mathrm{Tr}(\rho_{\mathrm{final}}\mathcal{T}(x_{3,n}, x_{3,0}; E; \psi_{n-1}, \ldots, \psi_0)\rho(x_{3,0}) \times \mathcal{T}^\dagger(x_{3,n}, x_{3,0}; E; \psi_{n-1}, \ldots, \psi_0)). \quad (11)$$

Equipped with this formula, the photon transition probability $P_{\gamma\gamma}$ is defined as the sum of the transition probabilities from an initially unpolarized pure photon state $\rho_{\mathrm{unpol}} = 1/2\,\mathrm{diag}(1, 1, 0)$ to the final polarization states $\rho_{11} = \mathrm{diag}(1, 0, 0)$ and $\rho_{22} = \mathrm{diag}(0, 1, 0)$:

$$P_{\gamma\gamma} = P_{11} + P_{22} = \mathrm{Tr}((\rho_{11} + \rho_{22})\mathcal{T}\rho_{\mathrm{unpol}}\mathcal{T}^\dagger). \quad (12)$$

## III. MAGNETIC FIELD CONFIGURATIONS AND SCENARIOS

When the photon/ALP beam propagates towards Earth, it crosses different regions of plasma and magnetic field configurations. The following environments are considered, ordered by increasing distance from Earth:

(1) The Galactic magnetic field of the Milky Way (GMF).
(2) The intergalactic magnetic field (IGMF).
(3) The magnetic field inside a galaxy cluster (intracluster magnetic field, ICMF) in the vicinity of the emitting source.

The observational evidence and model assumptions for each region are discussed in the following subsections. The goal is to find the magnetic field configuration—within current observational bounds—which results in a maximal photon-ALP mixing. In this way, a lower limit on $g_{a\gamma}$ can be derived.

### A. Magnetic field of the Milky Way

The regular component of the $B$ field of the Milky Way will be described with the analytical GMF model presented in Ref. [33]. The model consists of three components: a disk, a halo, and a so-called X component; and it predicts a field strength of the order $\mathcal{O}(\mu\mathrm{G})$. The model parameters were determined with a $\chi^2$ minimization, utilizing the data of the WMAP7 polarized synchrotron emission maps and Faraday rotation measurements of extragalactic sources. Compared to previous models (e.g., Ref. [34]), a relatively large field strength and extent is predicted for the halo and X component, which leads to a comparatively large conversion probability in certain regions in the sky. The turbulent component of the GMF is neglected here, since the typical coherence length is of the order of $\mathcal{O}(10\ \mathrm{pc})$, which is far smaller than the oscillation length of photon-ALP conversions. For each extragalactic VHE $\gamma$-ray source, the conversion probability is evaluated along the line of sight where it is assumed that the GMF is constant and homogeneous on a length scale of 100 pc. It was checked that smaller values for the domain length do not alter the results. Moreover, the density of the thermal electron plasma is calculated with the NE2001 code (in accordance with Ref. [33]), which predicts densities of the order of $10^{-1}\ \mathrm{cm}^{-3}$ [35]. For further details on the conversion in the GMF, see Ref. [31], where the same GMF model was utilized to compute the photon-ALP conversions.

### B. Intergalactic magnetic field

In contrast to the GMF, little is known about the intergalactic magnetic field. From the observational side, only upper limits exist on the field strength, which constrain the

IGMF at $z = 0$ to a few $10^{-9}$ G [36]; and, e.g., the authors of Ref. [37] find $B^0_{\rm IGMF} \equiv B_{\rm IGMF}(z = 0) \lesssim 6 \times 10^{-9}$ G for a coherence length of $\lambda^c_{\rm IGMF} = 50$ Mpc using Faraday rotation measurements of quasars. However, large-scale structure formation with magnetic field amplification and cosmic ray deflection simulations suggest smaller values, no larger than $B^0_{\rm IGMF} = 2 \times 10^{-12}$ G [38] or $B^0_{\rm IGMF} \approx 10^{-11}$ G in voids [39]. The morphology of the IGMF is not known either, and the most simple assumption is a domain-like structure, which is also adopted here. The field strength is constant in each cell and only grows with cosmic expansion, i.e., $B_{\rm IGMF}(z) = B^0_{\rm IGMF}(1 + z)^2$, but the orientation changes randomly from one cell to another. Furthermore, the domain length is given by $\lambda^c_{\rm IGMF}$. As shown in Ref. [27], adopting a Kolmogorov-type turbulence spectrum instead of the simple domain structure has negligible effects on the results. In principle, the same procedure is followed here as presented in Ref. [26], with the exception that the assumption of a strong mixing is dropped.

A scan over a logarithmic grid with $100 \times 100$ pixels in the $(\lambda^c_{\rm IGMF}, B^0_{\rm IGMF})$ space is performed to determine the most optimistic magnetic field setup. For each grid point, the photon survival probability is calculated with Eq. (12) for 5000 realizations of the orientation of $B_{\rm IGMF}$ for a fixed source distance $z = 0.536$, energy $E = 0.574$ TeV (this combination of $z$ and $E$ corresponds to an optical depth of $\tau = 4$ with the KD model), an ALP mass $m_a = 0.1$ neV, and two different values of the coupling. Only the conversion in the intergalactic magnetic field with absorption due to the EBL of the KD model is taken into account. The impact of the photon-ALP conversions is quantified with the boost factor $\mathcal{B}$, defined by

$$\mathcal{B} = \tilde{P}_{\gamma\gamma}/\exp(-\tau), \tag{13}$$

where $\tilde{P}_{\gamma\gamma}$ is the median of the distribution of photon survival probabilities [40]. The result is shown for two different values of the photon-ALP coupling in the top row of Fig. 1. As one would naively expect, for a large coupling of $g_{a\gamma} = 5 \times 10^{-11}$ GeV$^{-1}$ (top-right panel), the boost factor increases with increasing $B^0_{\rm IGMF}$ and increasing $\lambda^c_{\rm IGMF}$ up to a value of $10^{0.4} \approx 2.5$. For even higher values, the boost factor starts to decrease again and shows an oscillatory behavior. This feature was already observed in Ref. [26]: if the conversion probability becomes too high, the photon fraction in the beam is large at all times; but at the same time, the photon flux is attenuated by the interaction with the EBL. As a consequence, $\mathcal{B}$ declines, and one is tempted to choose the values of $\lambda^c_{\rm IGMF}$ and $B^0_{\rm IGMF}$ from within the 0.4 contour. The situation changes, however, if $g_{a\gamma}$ is decreased (top-left panel) by more than an order of magnitude to $10^{-12}$ GeV$^{-1}$. The entire region of $\mathcal{B} > 0$ is shifted towards higher values in the $(\lambda^c_{\rm IGMF}, B^0_{\rm IGMF})$ plane. Without any *a priori* assumption about values of the ALP mass and coupling, it is thus advisable to select the maximum values of $\lambda^c_{\rm IGMF}$ and $B^0_{\rm IGMF}$ that are allowed by observations, and we settle for $\lambda^c_{\rm IGMF} = \mathbf{50}$ Mpc and $B^0_{\rm IGMF} = 5$ nG. For the thermal electron density in the intergalactic medium, a typical value of $n_{\rm el,IGM} = 10^{-7}$ cm$^{-3}$ is adopted [41].

### C. Intracluster magnetic fields

In contrast to intergalactic magnetic fields, the existence of intracluster magnetic fields is well established. Synchrotron emission of the intracluster medium together with Faraday rotation measurements at radio frequencies have led to the common picture that turbulent magnetic fields of the order of $\mathcal{O}(\mu$G) fill the cluster volume (see, e.g., Refs. [42,43] for reviews and typical values of the model parameters used below). The turbulence is usually described with a Kolmogorov-type spectrum, or with the simpler cell-like structure which is again used here (as in Ref. [31]). There is evidence that the magnetic field strength follows the radial profile of the thermal electron distribution $n_{\rm el,ICM}$ in the cluster,

$$B_{\rm ICMF}(r) = B^0_{\rm ICMF}(n_{\rm el,ICM}(r)/n^0_{\rm el,ICM})^\eta, \tag{14}$$

with typical values $0.5 \lesssim \eta \lesssim 1$ and central magnetic fields up to $\sim 10$ $\mu$G in the most massive clusters. The thermal electron density is described by

$$n_{\rm el,ICM}(r) = n^0_{\rm el,ICM}(1 + r/r_{\rm core})^{-3\beta/2}, \tag{15}$$

with characteristic values of $\beta = 2/3$ and $r_{\rm core} = 200$ kpc. The coherence length is usually assumed to be comparable to galactic scales of the order of 10 kpc. As before, a grid scan over the $(\lambda^c_{\rm ICMF}, B^0_{\rm ICMF})$ plane is performed in order to determine the parameters that maximize the photon-ALP conversions. A cluster with a radius of 2 Mpc is assumed together with $\eta = 0.5$. Instead of the boost factor, the fraction of ALPs $P_{a\gamma}$ in the final state [i.e., $\rho_{\rm final} = \rho_{33} = (0, 0, 1)$] is shown in the bottom row of Fig. 1 for an initially unpolarized pure photon beam, $P_{a\gamma} = {\rm Tr}(\rho_{33}\mathcal{U}\rho_{\rm unpol}\mathcal{U}^\dagger)$. Again, 5000 $B_{\rm ICMF}$-field realizations are simulated, and the median $\tilde{P}_{a\gamma}$ is computed. The more ALPs leave the cluster, the stronger the effect will be on the VHE spectra, because more ALPs can convert back into photons in the GMF and enhance the observed flux. The bottom-left panel of Fig. 1 clearly shows that more ALPs are produced for stronger magnetic fields and longer coherence lengths for a photon-ALP coupling strength of $g_{a\gamma} = 10^{-11}$ GeV$^{-1}$. Interestingly, the conversion probability is constant for constant values of $B_0 \times \sqrt{L_{\rm coh}}$ (red dashed line), and $\tilde{P}_{a\gamma}$ increases quadratically with growing coupling strength until the maximum probability of $\sim 1/3$ is reached (bottom-right panel of Fig. 1). Not surprisingly, the maximum is reached for smaller couplings for larger values of $B_0 \times \sqrt{L_{\rm coh}}$. Thus, for an optimistic scenario, a central ICMF value of $B_0 = 10$ $\mu$G with a coherence

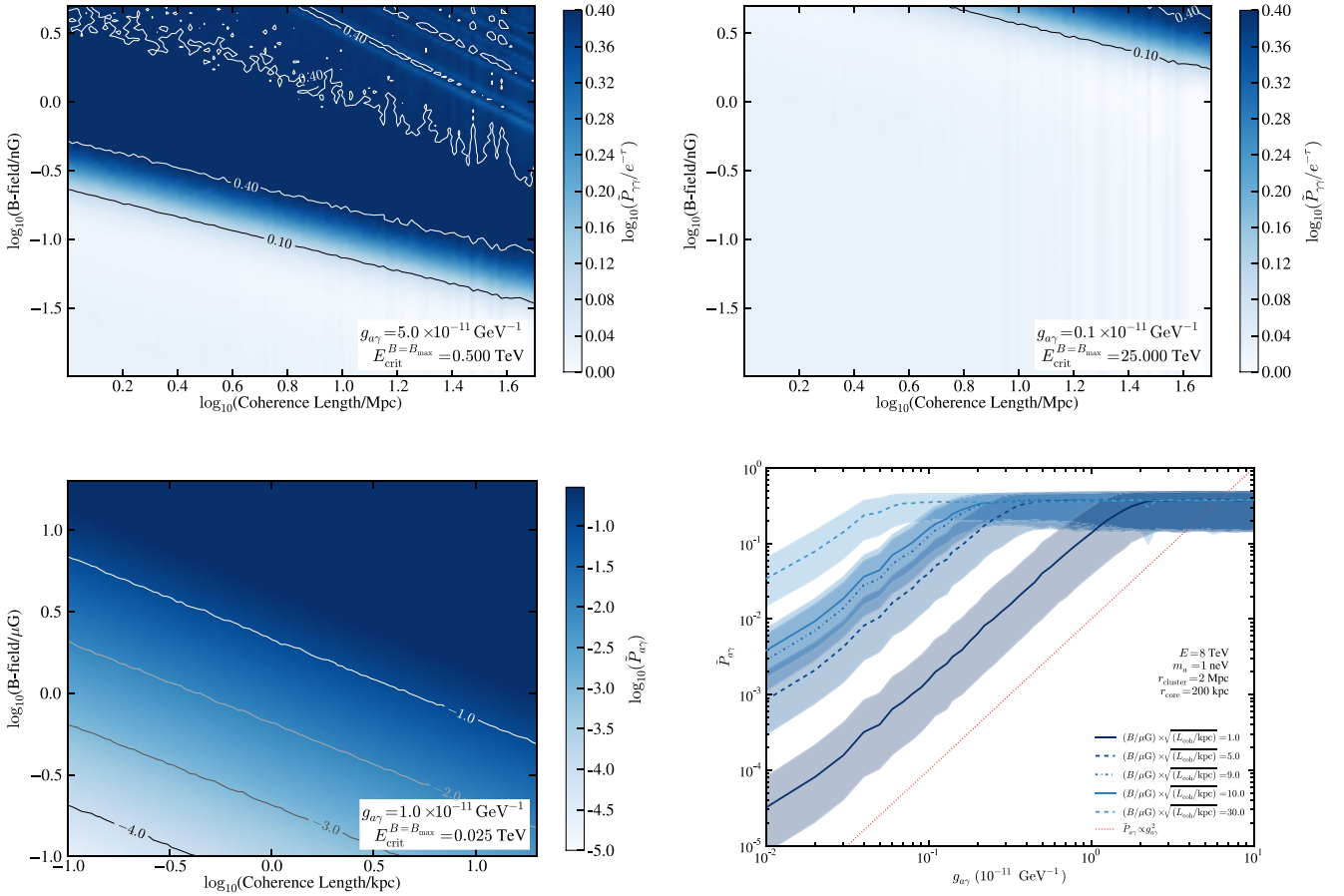


FIG. 1 (color online). Parameter space scan in the $(\lambda_c, B_0)$ plane. Top row: Photon-ALP conversion in the IGMF. The color map displays the boost factor of the median of all simulated $B_{\mathrm{IGMF}}$-field realizations; see Eq. (13). The adopted values for the coupling (Left column: large couplings; Right column: small couplings) are displayed in the figure together with the critical energy above which the conversion occurs in the strong mixing regime. Bottom row: Conversion in the ICMF. In the left panel, the color coding shows the fraction of the initial photon beam that is converted to ALPs (median over all realizations). The median of the conversion probability is constant for constant values of $B_0 \times \sqrt{L_{\mathrm{coh}}}$, as indicated by the red dashed line. The bottom-right panel displays the dependence of $\tilde{P}_{a\gamma}$ on the coupling $g_{a\gamma}$ for different values of $B_0 \times \sqrt{L_{\mathrm{coh}}}$. In this panel, 68% of all $B$-field realizations for each $B_0 \times \sqrt{L_{\mathrm{coh}}}$ value fall into the corresponding shaded regions. See text for further details.

length of 10 kpc is chosen, and it is assumed that the VHE-emitting AGN is located at the center of a galaxy cluster. The core thermal electron density is taken to be $n^0_{\mathrm{el,ICM}} = 10^{-2}$ cm$^{-3}$.

### D. Magnetic field scenarios

Now that the most optimistic values for the different magnetic fields are identified, four scenarios are presented for which the effect of photon-ALP oscillations on VHE $\gamma$-ray spectra will be investigated. In all four configurations, the conversion in the GMF is included.

(1) In the first scenario, called *general source* hereafter, no specific environment is assumed for the ALP production, and only the conversion in the GMF is included. Instead, an initial beam polarization $\rho_{\mathrm{init}} = 1/3\mathrm{diag}(e^{-\tau}, e^{-\tau}, 1)$ is considered. This situation corresponds to a maximal mixing in some turbulent magnetic field inside or around the source and a subsequent attenuation of the photon fraction of the beam. In this general scheme, one is not forced to apply some sort of averaging over the many possible orientations of the random magnetic field.

(2) In a second configuration, named *optimistic ICM*, it is optimistically assumed that *all* VHE $\gamma$-ray-emitting AGNs are located at the center of galaxy clusters of a 2 Mpc radius. The magnetic field changes over the distance from the cluster core as in Eq. (14) with a central magnetic field of $B^0_{\mathrm{ICMF}} = 10\ \mu$G and a coherence length of $\lambda^c_{\mathrm{ICMF}} = 10$ kpc. Any conversion in the intergalactic magnetic field is neglected, as well as any attenuation of the photon flux by local radiation fields inside the galaxy cluster. Upon exit of the galaxy cluster, the photon beam will be attenuated by the interaction with the EBL,

TABLE I. Model parameters for the different magnetic field scenarios. In frameworks including the conversion inside galaxy clusters, the beam is assumed to travel the distance $r_{\rm cluster}$ through the volume filled with a $B$ field. In the optimistic ICM scenario, the $B$ field varies as in Eq. (14). All AGNs are assumed to be located at the center of a cluster. In the fiducial case, the magnetic field and thermal electron density are assumed to be constant throughout the cluster volume. Only AGNs listed in Table 1 of Ref. [31] are assumed to lie within galaxy clusters. See text for further details.

| | IGMF | | | ICM | | | | | |
|---|---|---|---|---|---|---|---|---|---|
| Name | $B^0_{\rm IGMF}$ (nG) | $\lambda^c_{\rm IGMF}$ (Mpc) | $n^0_{\rm el,IGM}$ ($\times 10^{-7}$ cm$^{-3}$) | $B^0_{\rm ICMF}$ ($\mu$G) | $\lambda^c_{\rm ICMF}$ (kpc) | $r_{\rm cluster}$ (Mpc) | $n^0_{\rm el,ICM}$ ($\times 10^{-3}$ cm$^{-3}$) | $r_{\rm core}$ (kpc) | $\eta$ |
| General source | Only conversion in GMF, but $\rho_{\rm init} = 1/3{\rm diag}(e^{-\tau}, e^{-\tau}, 1)$ | | | | | | | | |
| Optimistic IGMF | 5 | 50 | 1 | ... | ... | ... | ... | ... | ... |
| Optimistic ICM | ... | ... | ... | 10 | 10 | 2 | 10 | 200 | 0.5 |
| Fiducial | 0.01 | 10 | 1 | 1 | 10 | 2/3 | 1 | ... | ... |

whereas the ALP fraction propagates unhampered over the entire distance to the Milky Way. In the GMF, ALPs and photons can again convert into each other. Apart from the ICMF that drops radially with distance from the cluster core, this is the same setup as investigated in Ref. [31].

(3) Thirdly, it will be assumed that no AGNs are affected by the photon-ALP conversion inside a galaxy cluster but, on the other hand, the intergalactic field will be taken to its most optimistic values, i.e., $B^0_{\rm IGMF} = 5$ nG and $\lambda^c_{\rm IGMF} = 50$ Mpc. This setup is labeled *optimistic IGMF* and is basically the same as that considered in, e.g., Ref. [26], apart from the complete energy-dependent treatment applied here.

(4) Finally, a set of more conservative model parameters is chosen to study the conversion in both the IGMF and ICMF. The parameters are conservative in the sense that they are not as close to the observational bounds as in the optimistic scenarios introduced above. Only the AGNs listed in Table 1 of Ref. [31] are assumed to be located inside a galaxy cluster. As their position relative to the cluster core is unknown, a constant ICMF of 1 $\mu$G is assumed. Furthermore, a value of $r_{\rm cluster} = 2/3$ Mpc is adopted as the distance that photons propagate through the intracluster medium [44]. The value of the IGMF is motivated by simulations of large-scale structure formations [38,39]. This framework will be called *fiducial*.

All scenarios are analyzed with two EBL models, namely the model of Ref. [9] (henceforth the FRV model) and the lower limit prediction of the KD model. The optical depth of the former is additionally scaled by a factor of $\sim$1.3, as suggested by recent studies of VHE $\gamma$-ray spectra [45]. These two EBL models more or less bracket the range of the EBL density allowed by lower limits from galaxy number counts mentioned in Sec. I and upper limits derived from VHE $\gamma$-ray spectra [13]. Moreover, it was shown in Ref. [46] that these two models result in the highest significance of the pair production anomaly; and it can be expected that comparably small photon-ALP couplings are able to reduce this tension significantly and, thus, to derive conservative lower limits on the photon-ALP coupling. The different scenarios and their corresponding model parameters are summarized in Table I. The photon-ALP conversion inside the source is not explicitly taken into account here, but a possible contribution is accounted for in the general source scenario.

## IV. PROBING THE OPACITY WITH VHE GAMMA-RAY SPECTRA

With the framework to calculate the photon survival probability $P_{\gamma\gamma}$ introduced in the previous sections, the observed VHE $\gamma$-ray spectra are corrected for absorption in the presence of ALPs. As it is not assumed that the photon-ALP conversions occur in the strong mixing regime, $P_{\gamma\gamma}$ can show a strong oscillatory behavior. Therefore, an observed spectral point with a flux $\Phi^{\rm obs}_i$ over an energy bin $\Delta E_i$ with central energy $E_i$ is corrected with an average transfer function,

$$\langle P_{\gamma\gamma}\rangle_i = \frac{1}{\Delta E_i}\int_{\Delta E_i} {\rm d}E P_{\gamma\gamma}(E), \tag{16}$$

so that the absorption corrected flux $\Phi_i$ is obtained by

$$\Phi_i = \langle P_{\gamma\gamma}\rangle_i^{-1}\Phi^{\rm obs}_i. \tag{17}$$

In practice, the photon survival probability is calculated for 40 energies for each source and linearly interpolated in $\log_{10}(E)$ and $\log_{10}(P_{\gamma\gamma})$. This has been cross-checked for one $(m_a, g_{a\gamma})$ pair with 100 energies, and the results are found to be compatible if only 40 energies are used.

The same technique as put forward in Appendix B of Ref. [18] is used here to quantify the significance of the pair production anomaly in the presence of ALPs. Each spectrum $j$ with data points that correspond to $\tau(z, E_i) \geq 2$,

TABLE II. List of VHE $\gamma$-ray spectra included in the analysis. The table shows the redshift of the source, the IACT experiment that measured it, the energy range covered by the spectrum, and the number of data points in the optical thick regime for the optical depth given by the KD model and by the scaled version of the FRV model.

| $j$ | Source | Redshift | Experiment | Energy range (TeV) | $N_{\tau\geq 2}$ ($\tau = 1 \times \tau_{\mathrm{KD}}$) | $N_{\tau\geq 2}$ ($\tau = 1.3 \times \tau_{\mathrm{FRV}}$) | Reference |
|---|---|---|---|---|---|---|---|
| 1 | Mrk 421 | 0.031 | HEGRA | 0.82–13.59 | 0 | 1 | [47] |
| 2 | Mrk 421 | 0.031 | HEGRA | 0.82–13.59 | 0 | 1 | [47] |
| 3 | Mrk 421 | 0.031 | H.E.S.S. | 1.12–17.44 | 0 | 2 | [48] |
| 4 | Mrk 421 | 0.031 | H.E.S.S. | 1.75–23.10 | 1 | 4 | [49] |
| 5 | Mrk 501[a] | 0.034 | HEGRA | 0.56–21.45 | 1 | 3 | [50] |
| 6 | 1ES 1950 + 650 | 0.048 | HEGRA | 1.59–10.00 | 0 | 1 | [51] |
| 7 | 1ES 1950 + 650 | 0.048 | HEGRA | 1.52–10.94 | 0 | 1 | [51] |
| 8 | PKS 2155-304[a] | 0.116 | H.E.S.S. | 0.23–2.28 | 0 | 2 | [52] |
| 9 | PKS 2155-304[a] | 0.116 | H.E.S.S. | 0.23–3.11 | 0 | 3 | [53] |
| 10 | PKS 2155-304[a] | 0.116 | H.E.S.S. | 0.22–4.72 | 0 | 6 | [54] |
| 11 | PKS 2155-304[a] | 0.116 | H.E.S.S. | 0.25–3.20 | 0 | 2 | [55] |
| 12 | RGB J0710 + 591 | 0.125 | VERITAS | 0.42–3.65 | 0 | 2 | [56] |
| 13 | H 1426 + 428 | 0.13 | HEGRA, CAT, WHIPPLE | 0.25–10.12 | 2 | 5 | [57] |
| 14 | 1ES 0229-200 | 0.140 | H.E.S.S. | 0.60–11.45 | 3 |  | [14] |
| 15 | H 2356-309 | 0.165 | H.E.S.S. | 0.18–0.92 | 0 | 1 | [58] |
| 16 | H 2356-309 | 0.165 | H.E.S.S. | 0.22–0.91 | 0 | 1 | [59] |
| 17 | H 2356-309 | 0.165 | H.E.S.S. | 0.23–1.71 | 0 | 1 | [60] |
| 18 | 1ES 1218 + 304 | 0.182 | VERITAS | 0.19–1.48 | 0 | 3 | [61] |
| 19 | 1ES 1101-232[a] | 0.186 | H.E.S.S. | 0.18–2.92 | 3 | 7 | [58] |
| 20 | 1ES 0347-121 | 0.188 | H.E.S.S. | 0.30–3.03 | 2 | 4 | [62] |
| 21 | RBS 0413[b] | 0.190 | VERITAS | 0.23–0.61 | 0 | 1 | [63] |
| 22 | 1ES 0414 + 009[a] | 0.287 | H.E.S.S. | 0.17–1.13 | 2 | 3 | [64] |
| 23 | 1ES 0414 + 009[a,b] | 0.287 | VERITAS | 0.23–0.61 | 0 | 1 | [65] |
| 24 | PKS 1222 + 21 | 0.432 | MAGIC | 0.08–0.35 | 0 | 1 | [66] |
| 25 | 3C 279[b] | 0.536 | MAGIC | 0.15–0.35 | 1 | 1 | [67] |
| 26 | 3C 279 | 0.536 | MAGIC | 0.08–0.48 | 1 | 2 | [15] |

[a]Assumed to be located in a galaxy cluster in the fiducial scenario (see Ref. [31], Table I).
[b]Not included in Ref. [18].

i.e., the optical thick regime, is fitted with an analytical function $f_j(E)$. A list with all considered spectra that fulfill this criterion is shown in Table II. The function $f_j(E)$ is either a power law or, in case the fit probability is $p_{\mathrm{fit}} < 0.05$, a logarithmic parabola,

$$f_j(E) = \begin{cases} N_0(E/E_0)^{-\Gamma}, & p_{\mathrm{fit}} \geq 0.05, \\ N_0(E/E_0)^{-(\Gamma+\beta_c \ln(E/E_0))}, & \text{otherwise}, \end{cases} \tag{18}$$

with flux and energy normalization $N_0$ and $E_0$, respectively; a power-law index $\Gamma$; and a curvature $\beta_c$. For each data point in the optical thick regime, the residual is calculated,

$$\chi_{ij} = \frac{\Phi_i - f_j(E_i)}{\sigma_i}, \tag{19}$$

which is normalized to the statistical measurement uncertainty $\sigma_i$ on the flux $\Phi_i$ (68% confidence). Under the hypothesis that $P_{\gamma\gamma}$ gives a correct prediction of the opacity of the Universe to VHE $\gamma$ rays, the residuals in the optical thick regime should follow a Gaussian distribution with zero mean. This conjecture is checked with the $t$ test, for which the variable

$$t = \frac{\bar{\chi}}{\sqrt{\sigma_\chi / N_\chi}}, \tag{20}$$

with $\bar{\chi}$ the mean and $\sigma_\chi$ the variance of the residual distribution that contains $N_\chi$ data points, follows a $t$ distribution from which the significance (one-sided confidence interval) can be calculated. This method to quantify the accordance between model and data has several advantages. Firstly, the functions to parametrize the spectra do not depend on any particular blazar emission model, as no constraints on the photon index $\Gamma$ nor on the curvature $\beta_c$ are made during the fit. Most spectra are adequately described by these functions, as shown in the Appendix. Secondly, no extrapolation from the optical thin to the optical thick regime is required, and the statistical uncertainties of the measurement enter the significance test self-consistently.

Without the contribution of ALPs, one finds for the spectra listed in Table II a significance of

$5.1 \times 10^{-6} \approx 4.4\sigma$ for the KD model and $2.1 \times 10^{-4} \approx 3.5\sigma$ for the FRV model scaled by 1.3 that the models do not describe the data. It might come as a surprise that the scaled FRV model gives a lower significance than the minimal attenuation model of Ref. [10]. The reason for this is that more data points migrate into the optical thick regime as the EBL density increases. This leads to an overall distribution closer to a zero mean and shows the limitation of the method: as long as the overall fit to all spectra is acceptable, the entire residual distribution must scatter around zero (see also Ref. [46]).

In the following discussion, ALPs are included in the correction of the observed spectrum. For this purpose, the transition probability for all four scenarios and the two different EBL models is calculated separately for each source listed in Table II. This is necessary because each AGN has a different redshift (important for the attenuation) and a different position in the sky (influencing the conversion in the GMF). Furthermore, $P_{\gamma\gamma}$ is computed over a grid of equally spaced values in the $(\log_{10}(m_a), \log_{10}(g_{a\gamma}))$ space. For the coupling constant, the range $10^{-13}$ GeV$^{-1} \leq g_{a\gamma} \leq 10^{-10}$ GeV$^{-1}$ is chosen for all magnetic field frameworks. The upper bound is motivated by the bound set by the CAST experiment of $g_{a\gamma} < 8.8 \times 10^{-11}$ GeV$^{-1}$ [68], while for the lower bound the contribution of ALPs is expected to become negligible. On the other hand, the range of the tested ALP masses differs in the different scenarios. It is determined by the critical energy given in Eq. (6) that should span an interval that includes the minimum and maximum energies of the VHE spectrum sample in Table II, namely 0.08 and 23.1 TeV. The different magnetic fields and thermal electron densities result in different mass ranges. For the general source and optimistic ICM configurations, a mass range of 1 neV $\leq m_a \leq 10^3$ neV is chosen; whereas for the optimistic IGMF setup, the smaller values of $B_{\rm IGMF}$ and the ambient density lead to a shift in the mass to $10^{-1.5}$ neV $\leq m_a \leq 10^{1.5}$ neV. In the combined fiducial scenario, it is settled for the intermediate range $10^{-0.5}$ neV $\leq m_a \leq 10^{2.5}$ neV. A resolution of the grid of $32 \times 32 = 1024$ points is selected in the particular ranges of $(\log_{10}(m_a), \log_{10}(g_{a\gamma}))$.

A complication is introduced by the random magnetic fields in the scenarios apart from the general source case. Since the exact orientation of the IGMF and ICMF in each domain is unknown, a large number $N_{\rm sim}$ of simulated random realizations is required. Here, $N_{\rm sim}$ will be set to 5000, and therefore, for each $(m_a, g_{a\gamma})$ pair, one ends up with 5000 values for the significance level of the $t$ test, $p_t$. One solution would be to compute the median (or mean) of the transfer function and afterwards calculate $p_t$. However, in the averaging process all information on the $p_t$ distribution is lost, and it is unclear if this certain value is statistically suitable to deduce a lower limit on $g_{a\gamma}$. Instead, the $p_t$ distribution is used to determine the $p_t$ value for which 95% of all $B$-field realizations result in a worse compatibility of the particular framework with the data (i.e., those realizations that result in a smaller $p_t$ value). This particular significance is henceforth denoted as $p_{95}$. In summary, for each scenario, one now has one $p_{95}$ value for each grid point in the $(m_a, g_{a\gamma})$ space. The lower limit on $g_{a\gamma}$ is then defined as the contour line for which $p_{95} = 0.01$. In this way, for $(m_a, g_{a\gamma})$ values below this contour line, 95% of all $B$-field realizations result in a compatibility of less than 1% with the data. For the two EBL models used here, this corresponds to a decrease of the significance of the pair production anomaly by a factor of $5.1 \times 10^{-4}$ (KD model) and $2.1 \times 10^{-2}$ (scaled FRV model).

## V. RESULTS

The results for the significance test introduced in the previous section are presented for each of the four scenarios developed in Sec. III. The upper panels of Fig. 2 show the $p_t$ values for the general source configuration for the KD model (top-right panel) and the FRV model (top-left panel). In this scenario, no random magnetic field is involved, and thus there is only one $p_t$ value for each pixel. The color coding and the contour lines show the $-\log_{10}(p_t)$ values and larger values of $p_t$ [smaller values of $-\log_{10}(p_t)$], which represent a higher probability that the corresponding $t$ value is the result of a statistical fluctuation; i.e., a higher probability that the transfer function is in accordance with the data. Clearly, the $p_t$ values increase with an increasing photon-ALP coupling. The lower limit on $g_{a\gamma}$ [$p_t = 0.01$ corresponds to the $-\log_{10}(p_t) = 2$ contour line] is $\sim 7.8 \times 10^{-11}$ GeV$^{-1}$ for the KD model and $\sim 1.4 \times 10^{-11}$ GeV$^{-1}$ for the FRV model, respectively, in the regime where the mixing becomes independent of the ALP mass at $m_a \lesssim 15$ neV. This mass marks the onset of the strong mixing regime (SMR) for all spectra in the environment of the Milky Way. For higher masses, the critical energy increases, and so does the number of spectral points outside the SMR. Higher couplings of $g_{a\gamma}$ are necessary to compensate this effect and to retain a low level of the significance of the pair production anomaly. Above $m_a \gtrsim 250$ neV, the tested coupling does not lead to a reduction of the tension between the model and data in comparison to the no-ALPs case. These observations are valid for both EBL models.

A similar overall behavior is found in the optimistic ICM case (Fig. 2, bottom-right panel: KD model; bottom-left panel: FRV model). The color code now displays the $p_{95}$ values for the 5000 simulated realizations of the random ICMF in each pixel. Apart from the overall trend, peculiar regions are visible for the contour lines. In certain mass ranges, the lower limit contour for $g_{a\gamma}$ extends down to almost $g_{a\gamma} = 10^{-12}$ GeV$^{-1}$ using the FRV model. These features are caused by the oscillatory

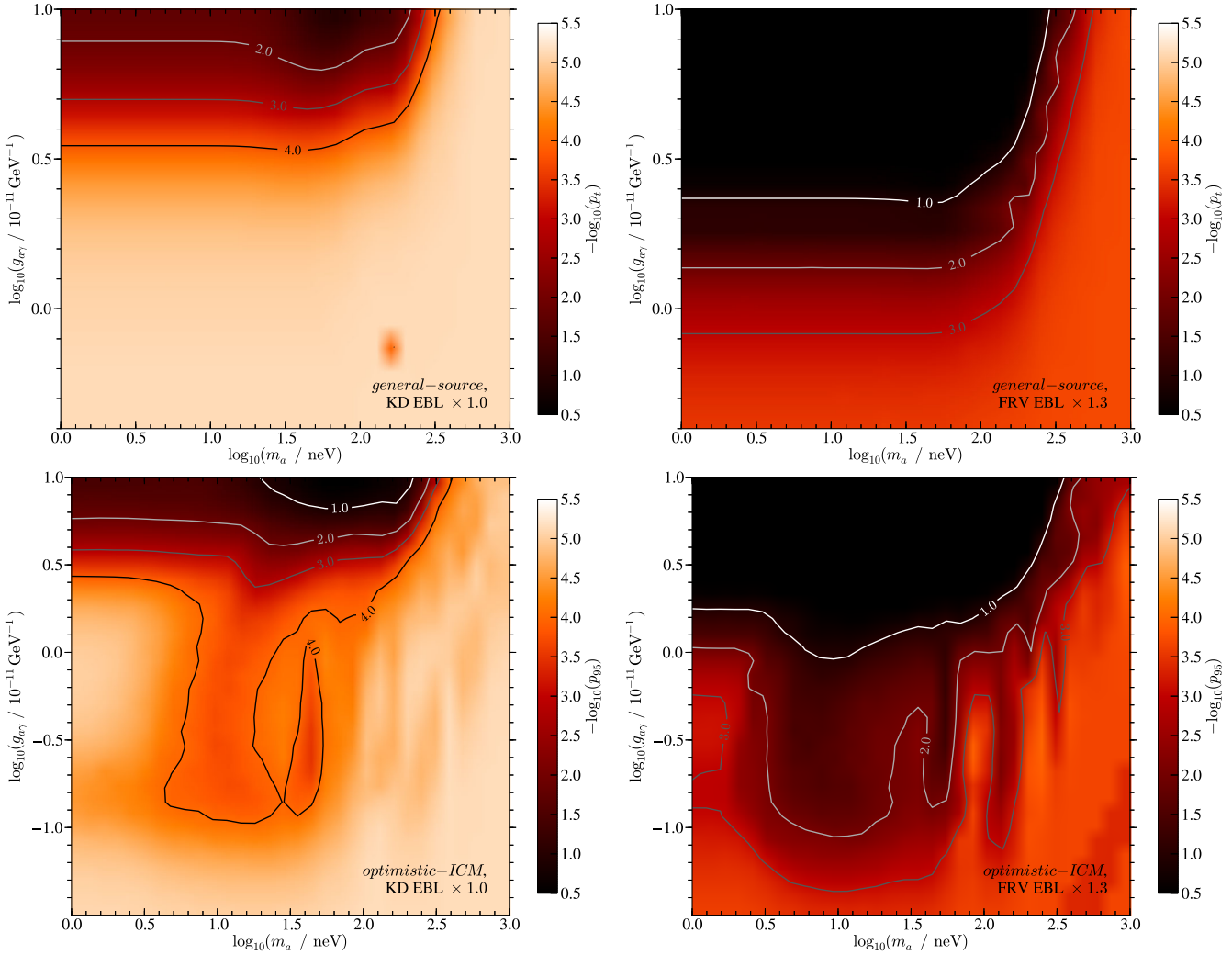


FIG. 2 (color online). Significance map for the photon-ALP conversion in the $(m_a, g_{a\gamma})$ plane. Smaller values (brighter regions) indicate less accordance between the model and the data. Upper panel: $p_t$ values for the general source scenario, shown as $-\log_{10}(p_t)$. Lower panel: $p_{95}$ values for the optimistic ICM case. For each pixel, 5000 realizations of the random magnetic field are simulated and $p_{95}$ is determined from the resulting 5000 $p_t$ values (cf. Sec. IV). In the left column, the attenuation due to the interaction of VHE $\gamma$ rays with the EBL is given by the KD model, whereas in the right column the FRV model is utilized. The maps are smoothed using a bilinear interpolation between the single $(m_a, g_{a\gamma})$ pixels.

behavior of $P_{\gamma\gamma}$ outside the SMR, which affects the low-energy data points in the spectra. These data points usually have the best count statistics, smallest error bars, and the strongest influence on the overall spectral fit. The oscillations in the transfer function can lead to a correction that is strong in one energy bin but small in the adjacent one. As a result, the spectral fit is altered and leads to residuals in the optical thick regime that are closer to zero for certain $(m_a, g_{a\gamma})$ pairs.

Thus, it is expected that these features will change if more VHE spectra are included in a future analysis. Furthermore, the oscillations of the transfer function lead to a poor fit quality for the spectra with the best overall statistics (Mrk 421 [49], Mrk 501 [50], and PKS 2155-304 [54]) and to a small overall fit probability (see the Appendix). This will lead to a broadening of the residual distribution and a possible overestimation of the $p_{95}$ values closer to 1. These features should not be taken as a preferred parameter region for ALPs to explain the opacity of the Universe.

In the optimistic IGMF scenario with the KD model, the only significant improvement over the no-ALP case is actually outside the SMR, as can be seen from Fig. 3 (top-right panel). Note that the mass range in which the transition to the SMR occurs has now shifted to lower masses due to the smaller IGMF and ambient electron density compared to the intracluster case. With the attenuation of the FRV model, the optimistic parameter choices for $B^0_{\rm IGMF}$ and $\lambda^c_{\rm IGMF}$ lead to a lower limit on $g_{a\gamma}$—as low as $\sim 3 \times 10^{-13}$ GeV$^{-1}$ (top-left panel of Fig. 3).

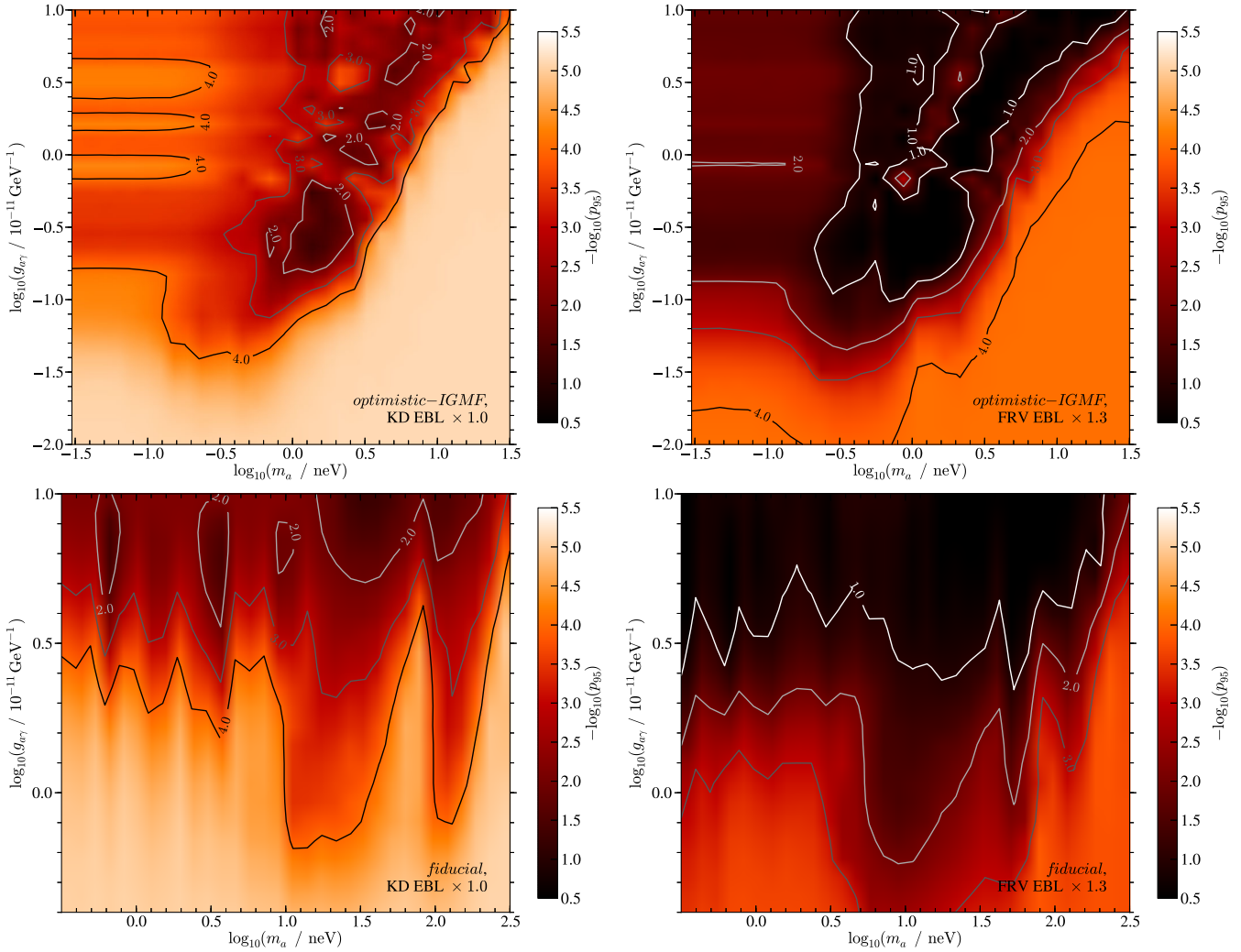


FIG. 3 (color online). Significance maps for the photon-ALP conversion. Same as the bottom row in Fig. 2, but for the optimistic IGMF scenario (top row) and fiducial case (bottom row).

The bottom row of Fig. 3 displays the results for the more conservative parameter choice of the fiducial framework. In this scenario, one cannot strictly speak about a lower limit on $g_{a\gamma}$, as neither the values of the magnetic fields nor the values for the coherence lengths are set to their observationally allowed upper limits. The $(m_a, g_{a\gamma})$ pairs that result in $p_{95} \geq 0.01$ can thus rather be seen as a preferred region in the parameter space if one tries to explain the opacity of the Universe with photon-ALP conversions. One has to keep in mind, though, that the majority of simulated $B$-field realization results in smaller $p_t$ values. Not surprisingly, one can conclude that the photon-ALP conversion in the IGMF is negligible, since the $p_{95} = 0.01$ contour line does not extend to lower values of $g_{a\gamma}$ at $m_a \approx 1$ neV, as observed in the optimistic IGMF case. Compared to the optimistic ICM case, the lower limit contour line has shifted towards higher values in $g_{a\gamma}$ because a smaller number of AGNs is assumed to be located inside galaxy clusters. However, it has to be underlined that ALPs are still able to improve the accordance of the model with the data significantly.

From Figs. 2 and 3, it is obvious that in the KD model, higher values of the photon-ALP coupling are necessary to reduce the tension between model and data below the threshold of $p_{95} = 0.01$ (more stringent lower limits) than in the scaled FRV model. The reason for this is twofold: On the one hand, without ALPs, the absorption correction in the FRV model is larger for high optical depths, which leads to higher residuals in some spectra. Lower photon-ALP couplings suffice in these cases to reduce the residuals. On the other hand, the significance of the pair production anomaly is lower in the scaled FRV model to begin with (cf. Sec. IV). Demanding the same decrease of significance as in the FRV model without ALPs to the lower limit value ($2.1 \times 10^{-4}$ to 0.01) in the KD model case results in a significance value of $\sim 2.4 \times 10^{-4}$,

close to the $p_t = 10^{-4}$ contour line. Especially in the optimistic IGMF and fiducial scenarios, this line is in good agreement with the $p_t = 10^{-2}$ contour line in the FRV model case.

VHE $\gamma$-ray spectra are subject to systematic uncertainties which can also affect the significance test used here. The authors of Ref. [18] identified several sources of uncertainties in the quantification of the significance of the pair production anomaly such as a selection bias of VHE sources, the uncertainty of the overall energy scale of IACTs, and spillover effects in the highest energy bins due to the limited energy resolution of IACTs (the reader is referred to Ref. [18] for a detailed discussion). Including these effects leads in general to a reduction of the significance. The strongest reduction, to $2.6\sigma$, was found if the last energy bins of all spectra were excluded from the analysis and the energy points were simultaneously scaled by $-15\%$ in energy (a conservative choice, as it was shown that a scaling of the order of 5% is in better agreement with a cross correlation between IACTs and the *Fermi*-LAT [69]). This certainly poses a lower limit on the significance, as it seems unlikely that all VHE spectra are influenced by these systematics in the same way. Nevertheless, a lower limit of $p_{95} = 0.01$ with the inclusion of ALPs would not help to significantly improve the accordance between model and data in this case of a marginal indication. If ALPs were required at all, higher photon-ALP couplings would be necessary. However, the goal here is to set lower limits on $g_{a\gamma}$ if the pair production anomaly is not explained by invoking all systematic uncertainties on the VHE observations at once.

Figure 4 compares the lower limits derived here with current observational upper limits, regions of theoretical interest, and sensitivities of planned experiments. Only the lower limits for the FRV model are shown, since they all lie below the limits derived with the KD model. The lower limits clearly extend below the stringent upper limits from the CAST experiment [68] (dark shaded region). In the optimistic IGMF case, they also lie below the upper limit derived from the nonobservation of prompt $\gamma$ rays from the supernova SN 1987a (gray shaded region) [70,71]. These $\gamma$ rays would be the result of ALPs reconverted in the GMF that are produced in the supernova explosion [72]. The dotted-dashed lines show theoretical upper limits on $g_{a\gamma}$ calculated from magnetic white dwarfs (mWDs) [73]. Photon-ALP conversions lead to a linear polarization $P_L$ of the photon beam [32], and by treating the current observations of mWDs as a limit, i.e., $P_L \lesssim 5\%$, one can derive a limit on the photon-ALP coupling. The different lines correspond to different values of the magnetic field strength of the mWDs and different values for the limit on $P_L$. Although the magnetic field and ambient density in the vicinity of mWDs are

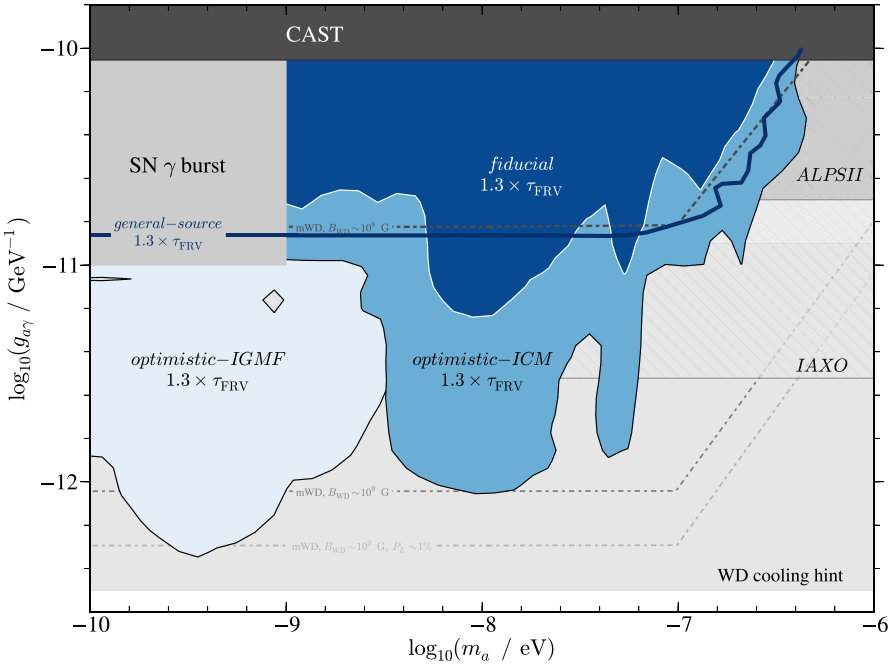


FIG. 4 (color online). ALP parameter space with the lower limits on $g_{a\gamma}$ derived in this paper. The lower limits for the different scenarios are displayed as blue shaded regions, or in the case of the general source scenario, as a dark blue solid line. They are only shown for the scaled FRV model, so that the optical depth is given by $\tau = 1.3 \times \tau_{\mathrm{FRV}}$. For comparison, upper limits, hints for theoretical preferred regions, and sensitivities of future experiments are also plotted. See text for further details.

very different from the scenarios considered here, the mWD considerations turn out to be sensitive in the same $(m_a, g_{a\gamma})$ region as the VHE observations. Nevertheless, the limits use a $B$-field model inferred from one single mWD. If they are confirmed with future observations, they will strongly constrain the parameter space for ALPs that can potentially decrease the opacity of the Universe for VHE $\gamma$ rays.

The lower limits of the optimistic scenarios extend into the preferred region for the ALP parameters to explain the white dwarf (WD) cooling problem. It is difficult with current theoretical models to satisfactorily reproduce the observed WD luminosity function. Including the production of ALPs, on the other hand, with a mass and coupling within the light-gray-shaded band in Fig. 4 [74] serves as an additional cooling mechanism for WD and can reduce the tension between current model predictions and data [75]. This issue is, however, subject to ongoing discussion [79].

Interestingly, the ALP parameter space of the fiducial scenario can be probed with planned experiments. The sensitivity forecasts for the improved Any Light Particle Search (ALPS II) [78,80] and the International Axion Observatory (IAXO) [81] are displayed as crosshatched and righthatched regions, respectively, in Fig. 4. The lower limits derived here thus pose an additional physics case for these future experiments.

## VI. SUMMARY AND CONCLUSIONS

In this article, VHE $\gamma$-ray observations have been used for the first time, to set lower limits on the photon-ALP coupling. Various magnetic field configurations have been considered, namely the magnetic field of the Milky Way, the intergalactic magnetic field, and the $B$ field that pervades the intracluster medium. Under the assumption of domainlike random $B$ fields, the photon-ALP conversion probability for different field strengths and coherence lengths is investigated. As a result, hypothetical ALPs from a large region of the $(m_a, g_{a\gamma})$ parameter space would be able to reduce the opacity of the Universe for VHE $\gamma$ rays and to ease the tension between the predictions of common EBL models and data from IACTs that has been found in Ref. [18]. If field strengths and the coherence lengths of the magnetic fields are assumed to be close to their maximally observationally allowed values, lower limits on $g_{a\gamma}$ are obtained that reach down to $g_{a\gamma} \sim 10^{-12}$ GeV$^{-1}$. Even lower values of $g_{a\gamma}$ could be obtained if, for instance, the GMF model were tuned to the most optimistic values allowed by the fitting errors calculated in Ref. [33]. Additional contributions to the GMF are also possible, such as a kiloparsec-scale magnetized wind [82] that could further enhance the conversion probability and reduce the lower limits. For more conservative values of the intervening $B$ fields, the limits are of the order of $g_{a\gamma} \gtrsim 2 \times 10^{-11}$ GeV$^{-1}$, close to the upper bounds of the CAST experiment and within the sensitivity estimates of future experiments such as ALPS II or IAXO.

Alternative mechanisms that are, in principle, able to increase the transparency of the Universe are also discussed in the literature. Active galactic nuclei could also be the source of cosmic-ray protons that produce secondary photons in the interaction with the EBL [83]. In such scenarios, the secondary photons are responsible for the high-energy end of VHE $\gamma$-ray spectra.

The effect of the unknown EBL density on the lower limits of $g_{a\gamma}$ has been assessed with two different EBL models. At the time being, the sample of VHE spectra is dominated by sources with a redshift $0.1 \lesssim z \lesssim 0.2$ and is thus most sensitive to changes in the EBL density at near-infrared wavelengths. As a consequence, certain EBL model realizations exist for which the pair production anomaly is less significant [46], and higher values of $g_{a\gamma}$ would be required to obtain a significant improvement over the situation without ALPs. One improvement would be to parametrize the EBL model independently (for instance, with splines, as done in, e.g., Ref. [13]) and recalculate the significances in the presence of ALPs. This is left for future investigations. Firm conclusions can only be drawn with future direct observations of the EBL and VHE measurements in the optical thick regime of both distant sources at several hundreds of GeV and nearby sources at several tens of TeV, which will also enable further tests of ALP scenarios. Several such observations have already been announced [84] and will become more feasible with the next generation of air shower experiments such as the Cherenkov Telescope Array [85], the High Altitude Water Cherenkov Experiment [86], and the Hundred*i Square-km Cosmic ORigin Explorer [87].

## ACKNOWLEDGMENTS

M. M. would like to thank the state excellence cluster "Connecting Particles with the Cosmos" at the University of Hamburg. The authors would also like to thank Alessandro Mirizzi and the anonymous referees for helpful comments improving the manuscript.

## APPENDIX: FIT QUALITIES

In this appendix, the quality of the fits of the analytical functions introduced in Eq. (18) is addressed. The fit statistics without the contribution of ALPs are listed in Table III. For both EBL models, all spectra show a high fit probability. The only exceptions are the spectra of Mrk 501 and one spectrum of 3C 279. The former spectrum is measured with high accuracy, resulting in very small statistical errors. It is dominated by its systematical uncertainties (see gray band in Fig. 10 in Ref. [50]), which are not included in the fit here. The spectrum of 3C 279 consists only of three data points, making a power law

TABLE III. List of fit qualities for all VHE $\gamma$-ray spectra if no ALPs are included in the deabsorption of the spectra. The table shows the $\chi^2$ values, the degrees of freedom (d.o.f.), and the resulting fit probabilities $p_{\rm fit}$ for both EBL models used here. See Table II for the references of each spectrum.

| $j$ | Source | Experiment | Fit function[a] | $\chi^2$ (d.o.f.) $\tau = 1 \times \tau_{\rm KD}$ | $p_{\rm fit}$ | $\chi^2$ (d.o.f.) $\tau = 1.3 \times \tau_{\rm FRV}$ | $p_{\rm fit}$ |
|---|---|---|---|---|---|---|---|
| 1 | Mrk 421 | HEGRA | LP | ... | ... | 4.10 (7) | 0.768 |
| 2 | Mrk 421 | HEGRA | PL | ... | ... | 8.75 (8) | 0.364 |
| 3 | Mrk 421 | H.E.S.S. | LP | ... | ... | 14.75 (10) | 0.142 |
| 4 | Mrk 421 | H.E.S.S. | LP, PL[b] | 16.97 (11) | 0.109 | 13.95 (12) | 0.304 |
| 5 | Mrk 501 | HEGRA | LP | 29.78 (14) | 0.008 | 38.55 (14) | 0.000 |
| 6 | 1ES 1950 + 650 | HEGRA | PL | ... | ... | 0.78 (3) | 0.854 |
| 7 | 1ES 1950 + 650 | HEGRA | PL | ... | ... | 7.89 (6) | 0.247 |
| 8 | PKS 2155-304 | H.E.S.S. | PL | ... | ... | 9.57 (7) | 0.215 |
| 9 | PKS 2155-304 | H.E.S.S. | PL | ... | ... | 8.34 (8) | 0.401 |
| 10 | PKS 2155-304 | H.E.S.S. | LP | ... | ... | 11.48 (14) | 0.648 |
| 11 | PKS 2155-304 | H.E.S.S. | PL | ... | ... | 5.46 (3) | 0.141 |
| 12 | RGB J0710 + 591 | VERITAS | PL | ... | ... | 2.00 (3) | 0.573 |
| 13 | H 1426 + 428 | HEGRA, CAT, WHIPPLE | PL | 9.06 (10) | 0.526 | 9.33 (10) | 0.501 |
| 14 | 1ES 0229-200 | H.E.S.S. | PL | 3.17 (6) | 0.787 | 3.86 (6) | 0.695 |
| 15 | H 2356-309 | H.E.S.S. | PL | ... | ... | 3.56 (6) | 0.735 |
| 16 | H 2356-309 | H.E.S.S. | PL | ... | ... | 4.20 (6) | 0.649 |
| 17 | H 2356-309 | H.E.S.S. | PL | ... | ... | 3.70 (6) | 0.717 |
| 18 | 1ES 1218 + 304 | VERITAS | PL | ... | ... | 2.33 (5) | 0.802 |
| 19 | 1ES 1101-232 | H.E.S.S. | PL | 5.70 (11) | 0.892 | 6.83 (11) | 0.813 |
| 20 | 1ES 0347-121 | H.E.S.S. | PL | 2.59 (5) | 0.763 | 2.30 (5) | 0.807 |
| 21 | RBS 0413 | VERITAS | PL | ... | ... | 0.02 (2) | 0.988 |
| 22 | 1ES 0414 + 009 | H.E.S.S. | PL | 1.86 (4) | 0.761 | 2.95 (4) | 0.567 |
| 23 | 1ES 0414 + 009 | VERITAS | PL | ... | ... | 0.51 (2) | 0.776 |
| 24 | PKS 1222 + 21 | MAGIC | PL | ... | ... | 0.24 (3) | 0.971 |
| 25 | 3C 279 | MAGIC | PL | 3.46 (1) | 0.063 | 3.95 (1) | 0.047 |
| 26 | 3C 279 | MAGIC | PL | 3.64 (3) | 0.303 | 4.48 (3) | 0.214 |
| *Combined* | | | | 76.25 (65) | 0.160 | 173.88 (165) | 0.303 |

[a]PL = power law, LP = logarithmic parabola.
[b]The spectrum is fitted with a logarithmic parabola in the KD model and with a power law in the FRV model, respectively.

the only meaningful fitting function. The combined $\chi^2$ values translate into satisfactory overall fit probabilities of $p_{\rm fit} = 0.160$ and $p_{\rm fit} = 0.303$ for the KD model and FRV model, respectively.

The fit qualities for the deabsorption of the observed VHE spectra with ALPs are poor in the transition to the strong mixing regime with $p_{\rm fit} \ll 1$. The corresponding high $\chi^2$ values are dominated by a few spectra only (as in the no-ALPs case), namely those with high count statistics and consequently small error bars. The largest contributions come from the spectra of Mrk 421 [49] and Mrk 501 [50], for the KD, and additionally, the spectrum of PKS 2155-304 [54] for the FRV. Again, these spectra are dominated by their systematic uncertainties, which are not included here.

The reason for the large contribution of these spectra to the total $\chi^2$ values is the oscillatory behavior outside the SMR. As a result of the oscillations, the fit residuals also scatter strongly around zero and give rise to a low fit probability. If the spectra with high statistics are removed from the samples, the $\chi^2$/d.o.f. values are close to one for all $(m_a, g_{a\gamma})$ values.

To summarize, the fits to most spectra in the $(m_a, g_{a\gamma})$ parameter space are acceptable. In the case of a small overall fit probability, the lower limits on $g_{a\gamma}$ are pushed towards lower values as the residual distribution broadens. Nevertheless, this bias mainly affects the region of ALP parameters outside the SMR and could be eliminated if the systematic uncertainties were included in the fit.

[1] A. I. Nikishov, Sov. Phys. JETP **393**, 14 (1962).
[2] J. V. Jelley, Phys. Rev. Lett. **16**, 479 (1966).
[3] R. J. Gould and G. Schréder, Phys. Rev. Lett. **16**, 252 (1966).
[4] M. G. Hauser, R. G. Arendt *et al.*, Astrophys. J. **508**, 25 (1998).
[5] M. G. Hauser and E. Dwek, Annu. Rev. Astron. Astrophys. **39**, 249 (2001).
[6] E. Dwek and F. Krennrich, arXiv:1209.4661.
[7] P. Madau and L. Pozzetti, Mon. Not. R. Astron. Soc. **312**, L9 (2000).
[8] G. G. Fazio, M. L. N. Ashby *et al.*, Astrophys. J. Suppl. Ser. **154**, 39 (2004).
[9] A. Franceschini, G. Rodighiero, and M. Vaccari, Astron. Astrophys. **487**, 837 (2008).
[10] T. M. Kneiske and H. Dole, Astron. Astrophys. **515**, A19 (2010).
[11] A. Domínguez, J. R. Primack *et al.*, Mon. Not. R. Astron. Soc. **410**, 2556 (2011).
[12] M. R. Orr, F. Krennrich, and E. Dwek, Astrophys. J. **733**, 77 (2011).
[13] M. Meyer, M. Raue, D. Mazin, and D. Horns, Astron. Astrophys. **542**, A59 (2012).
[14] F. Aharonian, A. G. Akhperjanian *et al.*, Astron. Astrophys. **475**, L9 (2007).
[15] J. Albert, E. Aliu *et al.*, Science **320**, 1752 (2008).
[16] A. de Angelis, M. Roncadelli, and O. Mansutti, Phys. Rev. D **76**, 121301 (2007).
[17] A. Mirizzi, G. G. Raffelt, and P. D. Serpico, Phys. Rev. D **76**, 023001 (2007).
[18] D. Horns and M. Meyer, J. Cosmol. Astropart. Phys. 02 (2012) 033.
[19] The effect of ALPs on various VHE spectra was also investigated by A. De Angelis, O. Mansutti, M. Persic, and M. Roncadelli, Mon. Not. R. Astron. Soc. **394**, L21 (2009).
[20] J. Jaeckel and A. Ringwald, Annu. Rev. Nucl. Part. Sci. **60**, 405 (2010).
[21] M. Cicoli, M. D. Goodsell, and A. Ringwald, J. High Energy Phys. 10 (2012) 146.
[22] R. D. Peccei and H. R. Quinn, Phys. Rev. Lett. **38**, 1440 (1977).
[23] S. Weinberg, Phys. Rev. Lett. **40**, 223 (1978).
[24] F. Wilczek, Phys. Rev. Lett. **40**, 279 (1978).
[25] A. Mirizzi and D. Montanino, J. Cosmol. Astropart. Phys. 12 (2009) 004.
[26] A. de Angelis, G. Galanti, and M. Roncadelli, Phys. Rev. D **84**, 105030 (2011).
[27] D. Wouters and P. Brun, Phys. Rev. D **86**, 043005 (2012).
[28] M. A. Sánchez-Conde, D. Paneque, E. Bloom, F. Prada, and A. Domínguez, Phys. Rev. D **79**, 123511 (2009).
[29] F. Tavecchio, M. Roncadelli, G. Galanti, and G. Bonnoli, Phys. Rev. D **86**, 085036 (2012).
[30] M. Simet, D. Hooper, and P. D. Serpico, Phys. Rev. D **77**, 063001 (2008).
[31] D. Horns, L. Maccione, M. Meyer, A. Mirizzi, D. Montanino, and M. Roncadelli, Phys. Rev. D **86**, 075024 (2012).
[32] G. Raffelt and L. Stodolsky, Phys. Rev. D **37**, 1237 (1988).
[33] R. Jansson and G. R. Farrar, Astrophys. J. **757**, 14 (2012).
[34] M. S. Pshirkov, P. G. Tinyakov, P. P. Kronberg, and K. J. Newton-McGee, Astrophys. J. **738**, 192 (2011).
[35] J. M. Cordes and T. J. W. Lazio, arXiv:astro-ph/0207156.
[36] P. P. Kronberg, Rep. Prog. Phys. **57**, 325 (1994).
[37] P. Blasi, S. Burles, and A. V. Olinto, Astrophys. J. Lett. **514**, L79 (1999).
[38] K. Dolag, D. Grasso, V. Springel, and I. Tkachev, J. Cosmol. Astropart. Phys. 01 (2005) 009.
[39] G. Sigl, F. Miniati, and T. A. Enßlin, Nucl. Phys. B, Proc. Suppl. **136**, 224 (2004).
[40] The median is preferred over the mean value, since the distribution of $P_{\gamma\gamma}$ is highly skewed (see Ref. [31]).
[41] N. Jarosik, C. L. Bennett, J. Dunkley *et al.*, Astrophys. J. Suppl. Ser. **192**, 14 (2011).
[42] F. Govoni and L. Feretti, Int. J. Mod. Phys. D **13**, 1549 (2004).
[43] L. Feretti, G. Giovannini, F. Govoni, and M. Murgia, Astron. Astrophys. Rev. **20**, 54 (2012).
[44] This value is motivated by the following reasoning: Assume that an AGN is placed randomly inside a sphere with a radius of 2 Mpc. One can compute the distance to the edge of the sphere in a certain direction. If this is repeated a large number of times, the median distance that a photon travels through the sphere is found to be approximately $2/3$.
[45] A. Abramowski, F. Acero, F. Aharonian *et al.* (H.E.S.S. Collaboration) (to be published).
[46] M. Meyer, D. Horns, and M. Raue, arXiv:1211.6405.
[47] F. Aharonian, A. Akhperjanian, M. Beilicke *et al.*, Astron. Astrophys. **393**, 89 (2002).
[48] *Proceedings of the 29th International Cosmic Ray Conference, Pune, India, 2005* edited by B. Sripathi Acharya, S. Gupta, P. Jagadeesan, A. Jain, S. Karthikeyan, S. Morris, and S. Tonwar (Tata Institute of Fundamental Research, Mumbai, 2005), Vol. 4, p. 319.
[49] M. Tluczykont, Proc. Sci., TEXAS2010 (2010) 197.
[50] F. A. Aharonian, A. G. Akhperjanian, J. A. Barrio *et al.*, Astron. Astrophys. **349**, 11 (1999).
[51] F. Aharonian, A. Akhperjanian, M. Beilicke *et al.*, Astron. Astrophys. **406**, L9 (2003).
[52] F. Aharonian, A. G. Akhperjanian, K.-M. Aye *et al.*, Astron. Astrophys. **430**, 865 (2005).
[53] F. Aharonian, A. G. Akhperjanian, A. R. Bazer-Bachi *et al.*, Astron. Astrophys. **442**, 895 (2005).
[54] F. Aharonian, A. G. Akhperjanian, A. R. Bazer-Bachi *et al.*, Astrophys. J. Lett. **664**, L71 (2007).
[55] F. Aharonian, A. G. Akhperjanian, G. Anton *et al.*, Astrophys. J. Lett. **696**, L150 (2009).
[56] V. A. Acciari, E. Aliu, T. Arlen, T. Aune *et al.*, Astrophys. J. Lett. **715**, L49 (2010).
[57] F. Aharonian, A. Akhperjanian, M. Beilicke *et al.*, Astron. Astrophys. **403**, 523 (2003).
[58] F. Aharonian, A. G. Akhperjanian, A. R. Bazer-Bachi *et al.*, Nature (London) **440**, 1018 (2006).
[59] F. Aharonian, A. G. Akhperjanian, A. R. Bazer-Bachi *et al.*, Astron. Astrophys. **455**, 461 (2006).
[60] A. Abramowski, F. Acero, F. Aharonian *et al.* (H.E.S.S. Collaboration), Astron. Astrophys. **516**, A56 (2010).
[61] V. A. Acciari, E. Aliu, T. Arlen, M. Beilicke *et al.* (VERITAS Collaboration), Astrophys. J. **695**, 1370 (2009).

[62] F. Aharonian, A. G. Akhperjanian, U. Barres de Almeida *et al.*, Astron. Astrophys. **473**, L25 (2007).
[63] E. Aliu, S. Archambault, T. Arlen *et al.*, Astrophys. J. **750**, 94 (2012).
[64] A. Abramowski, F. Acero, F. Aharonian *et al.* (H.E.S.S. Collaboration), Astron. Astrophys. **538**, A103 (2012).
[65] E. Aliu, S. Archambault, T. Arlen *et al.*, Astrophys. J. **755**, 118 (2012).
[66] J. Aleksić, L. A. Antonelli, P. Antoranz *et al.*, Astrophys. J. Lett. **730**, L8 (2011).
[67] J. Aleksić, L. A. Antonelli, P. Antoranz *et al.*, Astron. Astrophys. **530**, A4 (2011).
[68] S. Andriamonje, S. Aune, D. Autiero *et al.* (CAST Collaboration), J. Cosmol. Astropart. Phys. 04 (2007) 010.
[69] M. Meyer, D. Horns, and H.-S. Zechlin, Astron. Astrophys. **523**, A2 (2010).
[70] J. W. Brockway, E. D. Carlson, and G. G. Raffelt, Phys. Lett. B **383**, 439 (1996).
[71] J. A. Grifols, E. Massó, and R. Toldrà, Phys. Rev. Lett. **77**, 2372 (1996).
[72] The limits should be considered as an order of magnitude estimate, since they rely on some simplifications. For instance, a constant photon-ALP conversion probability in the GMF is assumed.
[73] R. Gill and J. S. Heyl, Phys. Rev. D **84**, 085001 (2011).
[74] Reference [75] sets bounds on the mass of the QCD axion or, equivalently, on the electron-axion coupling. This can be translated into a bound on the photon-axion coupling [76,77], and consequently on the photon-ALP coupling. The values shown here are taken from Ref. [78].
[75] J. Isern, E. García-Berro, S. Torres, and S. Catalán, Astrophys. J. Lett. **682**, L109 (2008).
[76] G. G. Raffelt, Lect. Notes Phys. **741**, 51 (2008).
[77] J. Redondo (private communication).
[78] J. L. Hewett, H. Weerts, R. Brock, J. N. Butler, B. C. K. Casey, J. Collar, A. de Gouvea, R. Essig, Y. Grossman, W. Haxton *et al.*, arXiv:1205.2671.
[79] B. Melendez, M. M. Bertolami, and L. Althaus, arXiv:1210.0263.
[80] ALPS II Collaboration, "ALPS II Technical Design Report" (to be published).
[81] I. G. Irastorza, F. T. Avignone, S. Caspi *et al.*, J. Cosmol. Astropart. Phys. 06 (2011) 013.
[82] J. E. Everett, E. G. Zweibel, R. A. Benjamin, D. McCammon, L. Rocks, and J. S. Gallagher III, Astrophys. J. **674**, 258 (2008).
[83] W. Essey and A. Kusenko, Astropart. Phys. **33**, 81 (2010).
[84] For example, the detection of the distant BL Lac KUV Report No. 00311-1938 with H.E.S.S. and the observation of a flaring state of Markarian 421 with VERITAS were recently announced; see http://tevcat.uchicago.edu/.
[85] M. Actis, G. Agnetta, F. Aharonian, A. Akhperjanian, J. Aleksić, E. Aliu, D. Allan, I. Allekotte, F. Antico, L. A. Antonelli *et al.*, Exp. Astron. **32**, 193 (2011).
[86] G. Sinnis, A. Smith, and J. E. McEnery, in *The Tenth Marcel Grossmann Meeting: On Recent Developments in Theoretical and Experimental General Relativity, Gravitation and Relativistic Field Theories*, edited by M. Novello, S. Perez Bergliaffa, and R. Ruffini (World Scientific, Singapore, 2006), p. 1068.
[87] M. Tluczykont, D. Hampf, D. Horns, T. Kneiske, R. Eichler, R. Nachtigall, and G. Rowell, Adv. Space Res. **48**, 1935 (2011).